Ultrasound in Med. & Biol., Vol. 29, No. 8, pp. 1193–1204, 2003

0301-5629/03/$–see front matter

ELSEVIER

doi:10.1016/S0301-5629(03)00064-4

● *Original Contribution*

THE COOLING EFFECT OF LIQUID FLOW ON THE FOCUSSED ULTRASOUND-INDUCED HEATING IN A SIMULATED FOETAL BRAIN

GILBERT J. VELLA,* VICTOR F. HUMPHREY,† FRANCIS A. DUCK‡ and STANLEY B. BARNETT§
*School of Biomedical Sciences, The University of Sydney, Sydney, Australia; †School of Physics, University of Bath, Bath, UK; ‡Medical Physics Department, Royal United Hospital Bath, Bath, UK; and §CSIRO Telecommunications & Industrial Physics, Sydney, Australia

(*Received* 11 *September* 2002; *revised* 5 *February* 2003; *in final form* 12 *February* 2003)

Abstract—There is a need to investigate the thermal effects of diagnostic ultrasound (US) to assist the development of appropriate safety guidelines for obstetric use. The cooling effect of a single liquid flow channel was measured in a model of human foetal brain and skull bone heated by a focussed beam of simulated pulsed spectral Doppler US. Insonation conditions were 5.7 μs pulses, repeated at 8 kHz from a focussed transducer operating with a centre frequency of 3.5 MHz, producing a beam of −6 dB diameter of 3.1 mm at the focus and power outputs of up to 255 ± 5 mW. Brain perfusion was simulated by allowing distilled water to flow at various rates in a 2 mm diameter wall-less channel in the brain soft tissue phantom material. This study established that the cooling effect of the flowing water; 1. was independent of the acoustic source power, 2. was more effective close to the flow channel, for example, there was a marked cooling at a distance of 1 mm and negligible cooling at a distance of 3 mm from the channel; and 3. initially increased at low flow rates, but further increase above normal perfusion had very little effect. (E-mail: G.Vella@fhs.usyd.edu.au) © **2003 World Federation for Ultrasound in Medicine & Biology.**

Key Words: **Pulsed ultrasound, Phantom, Fetus, Liquid flow, Bone heating, Hyperthermia, Focussed ultrasound beam.**

INTRODUCTION

The importance of investigating thermal effects of diagnostic ultrasound (US) to assist the development of appropriate safety guidelines for obstetric use is well established (Barnett 2000).

B-mode grey-scale imaging is the most commonly used form of diagnostic US in obstetrics. A scanned beam interrogates tissues with US for only a short time (short dwell time), resulting in negligible thermal risk to the fetus or the mother (Barnett 1996). However, pulsed Doppler mode, used to measure the real-time movement of blood flow in arteries, may use higher acoustic outputs (Henderson et al. 1995; Duck and Henderson 1998) directed at a fixed volume of tissue for dwell times of at least 2 min (Andrews et al. 1987). Such exposures have the potential to significantly heat tissues that have a very high US absorption coefficient, such as bone, from which heat is dispersed to adjacent soft tissue. *In vitro* animal studies have shown that, using acoustic outputs close to the maximum from commercial pulsed Doppler units, temperature elevations of over 5°C are possible in brain tissue adjacent to foetal skull bone (Barnett 2001). This temperature elevation is well above the threshold of 1.5°C considered safe for foetal application by the World Federation of Ultrasound in Medicine and Biology (Barnett 1998). In obstetrics, pulsed Doppler is used clinically to measure intracranial arterial flows in the foetal brain (McCowan and Duggan 1992).

It is generally accepted that blood flow through live tissue (perfusion) will reduce these temperature elevations by convecting heat away from the tissue (Shaw et al. 1996). The conditions and extent to which perfusion provides cooling are still not fully understood, and are the focus of the present study.

Modern ultrasonic scanners incorporate a real-time output display standard, ODS, (AIUM/NEMA 1992), which uses a thermal index (TI) and a mechanical index (MI) as indicators of the potential thermal and mechanical bioeffects during an examination (Abbott 1999). The TI represents an estimate of the maximum worst-case

Address correspondence to: Gilbert J. Vella, School of Biomedical Sciences, The University of Sydney, P. O. Box 170, Lidcombe NSW 1825 Australia. E-mail: G.Vella@fhs.usyd.edu.au

Table 1. Summary of animal perfusion studies using narrow us beams

Investigators	Animal species	Exposure time (s)	−6 dB beam width (mm)	Intensity I_{SPTA} (W cm^{-2})	% cooling
Carstensen et al. (1990)	adult mouse	90	2.8	1.5	12%
Horder et al. (1998b)	late-gestational-age guinea pig at parietal bone	120	2.6	2.8	12%
Horder et al. (1998a)	late-gestational-age guinea pig at sphenoid bone	120	2.6	2.8	25%
Duggan et al. (2000)	neonatal pig	90	3.0	1.5	0%

temperature rise in tissue based on calculations using a number of simple tissue-heating models. Although perfusion was included in the formulation of the TI algorithms, its precise nature is still not known so as to adequately replicate its complexity.

A consideration of these important safety implications has instigated a number of animal studies that have assessed the effects of blood flow on the US-induced heating in foetal skull bone. This was determined by measuring the temperature elevation in the skull during ultrasonic exposure when the animal was alive and repeated immediately after the animal was euthanised. The difference in the maximum temperature rise reached in the skull bone gave a measure of the cooling due to perfusion. Although narrow and wide US beams are used in clinical practice, the present study will report only on the cooling effects of a liquid flowing near skull bone heated by narrow US beams. The effect of the liquid flow on bone heated by wide beams is considered in a companion paper (Vella et al. 2003). A number of *in vivo* studies using narrow ultrasonic beams have been reported in which the effects of perfusion on ultrasonically heated animal skull bone were measured (Table 1). The measurements reveal a large variation in the perfusion-induced cooling, ranging from zero to 25% cooling, depending on the animal species, location at which the temperature was measured and the ultrasonic conditions. Based on these data, we hypothesised that a key factor in the variability in the perfusion-induced cooling in these experiments was the location of the heated bone site and its proximity to the perfusing channels. There is strong supporting evidence for this hypothesis from the perfusion-induced cooling effects detected when using hyperthermia to treat tumours. Theoretical studies by Lagendijk (1982), Billard et al. (1990), Crezee and Lagendijk (1992) and Kolios (1996), as well as experimental studies by Hume et al. (1979), Dorr and Hynynen (1992), and Kolios et al. (1999) have clearly established that large blood vessels can produce steep temperature gradients and a significant cooling effect, leading to underdosage of the tumour during hyperthermia. This underdosage is believed (Lagendijk 1982) to be the main reason for tumour regrowth after a dramatic regression when treated solely by hyperthermia.

Measurements in an isolated fixed porcine kidney (Kolios et al. 1999) with distilled deionised water as the perfusate showed that, even for very short treatment times (3 to 20 s), large vessels can have significant cooling effects on the temperature distribution in tissue. This was particularly evident for vessels closer to the heated tissue.

Dorr and Hynynen (1992) measured the effect of blood flow on the temperature rise *in vivo* of ultrasonically heated thigh muscles in greyhound dogs. A vascular occluder and Doppler flow probe were placed on the femoral artery (approximately 5 mm diameter) to control and monitor blood flow. Temperatures were measured and compared for the cases when the thigh muscles were exposed to US for 2 min with no blood flow in the femoral artery and then with normal blood flow. Measurements revealed that the perfusion-induced cooling was dependent on how close the femoral artery was to the heated muscle tissue. Normal blood flow produced a 75% cooling in the thigh muscles directly below the femoral artery, which reduced to 31% cooling at 9 mm from the femoral artery.

The variability in the perfusion-induced cooling measured in the animal skull bone experiments is difficult to adequately explain due to the different sites at which the temperature was measured and the different bone sizes (and consequent ultrasonic absorption). Hence, it is desirable to use a simple and reproducible skull bone/brain tissue phantom to investigate the dependence of the cooling effect of liquid flow on a number of important factors, one of which has already been hypothesised. At the outset, it is important to note the limitations of this phantom. Given the complexity in the development of connective tissue and neuromuscular elements within the human fetus, this phantom cannot accurately reproduce *in vivo* perfusion conditions. Brain perfusion was simulated by liquid flow in a single channel within the phantom.

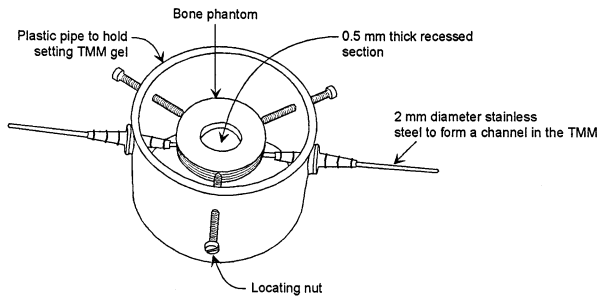

Fig. 1. A schematic diagram of the laboratory constructed bone phantom being supported in a plastic pipe just before it is filled with tissue-mimicking material (described below). The stainless-steel rod is in position so as to form the channel in the tissue-mimicking material.

The aim of the present study was twofold: 1. To fabricate a simple test phantom designed to simulate the absorbing material of a human foetal skull bone and adjacent brain tissue; 2. to measure the cooling effect of water flowing at a steady rate in a channel or simulated "arterial vessel" near a heated skull-bone target in the test phantom, using a narrow US beam, as a function of flow rate, acoustic source power and bone-channel separation distance.

MATERIALS AND METHODS

Phantom preparation

A number of test phantoms have been developed to validate the use of pulsed Doppler systems for the measurement of blood flow (Law et al. 1989). These were designed with the special requirements of Doppler in mind (*i.e.*, appropriate scattering properties of the blood-mimicking liquid flowing in a tube material of similar acoustic impedance to the blood-mimicking liquid). The requirements for the current study are quite different because it is necessary to match the thermal properties of blood with those of the flowing liquid. In addition, the vessel walls must have similar ultrasonic absorption properties to soft tissue, so that no additional heating is produced when the phantom is exposed to US.

The vascular-mimicking phantom was formed in a rigid plastic pipe (75 mm internal diameter and 3 mm thick wall) containing a human foetal-bone mimic immersed in a soft tissue-mimicking material through which a flow channel was formed (Fig 1). The soft tissue-mimicking material (T-MM) was made from a National Physical Laboratory formulation (Bacon and Shaw 1993) based on an animal gelatine and water mixture first used by Madsen et al. (1982) and later improved by Wu et al. (1992). An estimate of the foetal brain mass in the third trimester stage was calculated from measurements of the biparietal diameter (England 1996; Bettelheim et al. 1997) and brain density (Duck 1990). This estimate of 175 g, used as the mass of T-MM for the phantom in the present study, accords with an experimental study that measured the third trimester foetal brain mass to be 160 ± 19 g (Schultz et al. 1962).

The skull-bone mimic was made from a high-density polyethylene (DSM Engineering Plastic Products Limited, Redditch, UK) that has very similar thermal and ultrasonic properties to those of human foetal bone (Pay et al. 1998). Pay and colleagues note that, although the attenuation coefficient of the high-density polyethylene (2 dB cm^{-1} MHz^{-1}) is lower than would be expected for human foetal bone (5 dB cm^{-1} MHz^{-1}), the thermal conductivity and diffusivity are better matched to the ideal values for human foetal bone. The bone-mimic material used in this study had a thermal conductivity of 0.42 W m^{-1} K^{-1} (Product details, RS Components Ltd, Corby, UK) compared with the estimated range for foetal bone of 0.45 to 0.55 W m^{-1} K^{-1} (Pay et al. 1998). Similarly, the thermal diffusivity of the bone-mimic material of 2.5×10^{-7} m^2 s^{-1} (Product details, RS Components Ltd) compares well with the estimated range for foetal bone of 1.7 to 2.5×10^{-7} m^2 s^{-1} (Pay et al. 1998). These thermal parameters are more important in determining the US-induced temperature rise in the bone mimic.

The extent of the ultrasound reflections at the bone-mimic surface depends on the relative values of acoustic impedances for the bone mimic and the surrounding tissue. The acoustic impedance of the bone-mimic material was 2.1×10^6 rayls (Product details, RS Components Ltd.), which is within the estimated range of values for ideal foetal bone of 2.1×10^6 to 4.3×10^6 rayls (Pay et al. 1998). A thickness of 0.5 mm was chosen to simulate the foetal skull bone because the thickness of the human foetal parietal bone is 0.54 mm at term (Ohtsuki 1977). The skull-bone phantom was formed by machining a 0.5 mm thick recessed section from a 40 mm diameter disk of high density polyethylene. Small grooves were formed on the sides of the disk so that it could be supported by three brass screws at various separations from the flow channel.

The phantom was connected to the flow system by sturdy tapered barbed polypropylene connectors (Fisher Scientific UK, Leicestershire, UK) that were glued to the outside ends of the plastic pipe. One option for guiding the flow in the tissue-mimicking material was to use rigid tubing, such as plastic or rubber, as employed in many phantoms devised to measure blood flows using Doppler US (Law et al. 1989). However, such materials have a high acoustic attenuation and would cause additional heating in the wall material when exposed to US. Consequently, a wall-less channel design (based on the type by Rickey et al. 1995) was chosen, in preference to the

rigid material method, to avoid any possible artefactual heating.

The wall-less channel was formed by sliding a stainless-steel rod of diameter 2.0 mm inside the barbed plastic connectors at set distances from the bone mimic (Fig 1). After the lower end of the plastic pipe was sealed with cling film, the tissue-mimicking material, while still liquid, was poured into it and allowed to set while in a desiccator maintained at 5°C. After a week, the stainless-steel rod was carefully removed to leave a well-defined wall-less channel of diameter 2 mm. The choice of a 2-mm diameter channel was made because the diameters of the intracerebral vessels in the human fetus are about 1 mm to 3 mm (Seibert et al. 1990; Lewinsky et al. 1991). This simple channel simulated some of the major arterial vessels close to the skull bone, such as the superficial branches of the major cerebral and meningeal arteries (Moore and Dalley 1999).

The temperature of the skull-bone mimic was measured using 50 μm K-type chromel-alumel thermocouples attached to the upper and lower surfaces of the bone mimic. The upper surface of the bone mimic simulates the outer aspect of the skull bone (*i.e.*, proximal to the transducer and where the thermal index for bone, TIB, is estimated). The lower surface (distal to the transducer) replicates the more important biologic site, the inner surface of a foetal skull in contact with brain tissue. The thermocouple junctions were positioned and fixed to the centre of the bone mimic with a small drop of superglue (Ultrafast Cyanoacrylate, RS Components Ltd.). The thermocouple output was measured by a HP 34420A nanovoltmeter (Agilent Technologies, Palo Alto, CA), with a distilled water ice bath for the cold reference junction, which detected the temperature at 1-s intervals and downloaded the values into a personal computer *via* an RS232 cable connector. Temperature measurements were made with an overall precision of 0.05°C.

The use of superglue to attach the thermocouples to the bone phantom was essential to ensure correct positioning and good contact with the bone phantom. Measurement artefacts may be associated with the measurement of temperature using thermocouples during ultrasonic exposure (Waterman et al. 1991). They arise from four possible sources: 1. viscous heating; 2. reflection and scattering of the US waves from the thermocouple; 3. absorption heating due to any plastic coating; and 4. heat conduction along the thermocouple wires. The first three sources will cause the recorded temperature to be higher than the actual temperature, and the conduction artefact tends to underestimate the actual temperature (Waterman et al. 1991).

Viscous heating is the additional temperature rise due to the vibration of the thermocouple probe relative to the surrounding medium (Fry and Fry 1954). This viscous heating error is reduced proportionally as the thermocouple diameter is reduced compared with the ultrasonic beam width (Goss et al. 1977) and is considered to be a minimum for bare thermocouple wires of 50 μm diameter or less (Waterman et al. 1991). The use of 50 μm diameter thermocouples in the present study would, thus, have produced minimal viscous effects, as was experimentally confirmed by Doody et al. (1999), who also used such diameter thermocouples in a study of ultrasonically induced heating in foetal vertebrae.

The artefact from reflection and scattering of US waves is minimised if the diameter is less than the wavelength (Waterman et al. 1991). The wavelength in the soft tissue-mimicking material in this study would have been 430 μm; in the bone-mimicking material, it would have been 650 μm. Because these wavelengths are so much larger than the 50 μm thermocouple wires used in this study, very little influence would be expected from this artefact.

The absorption artefact, caused by the additional heating of any plastic coating on the thermocouple, is strongly dependent on the actual material coating (Martin and Law 1983; Kuhn and Christensen 1986). Although the drop of superglue would have introduced an absorption artefact, it would have also minimised the viscous artefact as the thermocouple probe was secured to the bone mimic. In any event, the main focus of the present study was the calculation of the cooling effect due to fluid flow in a phantom, which essentially involves the ratio of two temperatures; one with and the other without fluid flow. Hence, the identical artefact for both temperatures would produce a negligible overall error in the cooling effect. The effect of the absorption artefact on the absolute temperature will be given in the Results section.

The conduction artefact occurs because the metal thermocouple wires have a greater thermal conductivity than tissue, and heat is lost along the wires as it flows down the temperature gradient from high to low temperature (Dickinson 1985; Waterman et al. 1991). This is negligibly small in this case because the chromel and alumel wires are so small (50 μm) and their thermal conductivities (Bentley 1998) are much lower than copper of the same size, if one were using a copper–constantan (T-type) thermocouple.

Flow system

Thin-walled plastic tubing (Fisher Scientific) was slipped over the tapered barbed polypropylene connectors to be linked with the flow system. Distilled water was chosen as the flowing liquid because its thermal properties (such as specific heat and thermal conductivity) are similar to those of blood (Duck 1990). Although a better thermal match to blood can be achieved with a

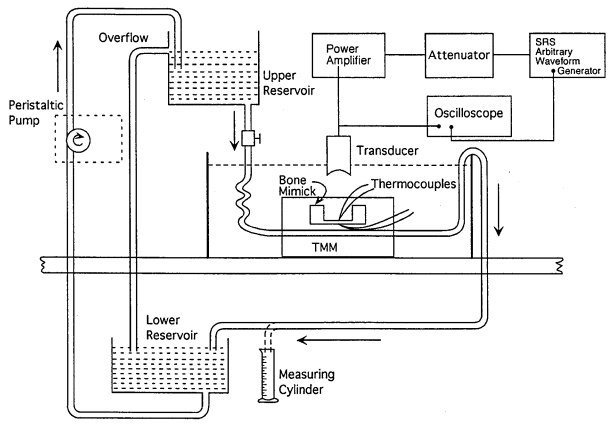

Fig. 2. The complete experimental arrangement showing the bone/brain phantom, flow circuit and the US insonation systems.

glycerol and water mixture, the relative simplicity of using water alone, without the need for continual mixing of the glycerol/water mixture encouraged the use of water as the flowing liquid.

The skull bone/brain tissue phantom was placed in a 25-litre glass tank containing distilled water (Fig 2). Adjusting the height between the upper and lower reservoirs of the gravity-fed system set the constant flow rate through the phantom. A peristaltic pump (Watson Marlow, Cheltenham, UK) pumped water from the lower reservoir to the upper reservoir. An overflow pipe in the upper reservoir ensured that a constant level was maintained in that reservoir. The constant flow rate was measured by diverting the flow, which entered the lower reservoir, into a measuring cylinder for a known time.

Two precautions were taken with the flow system. The first ensured that the temperature of the water entering the perfusing channel within the phantom was the same as the phantom temperature. This was achieved by allowing the water from the upper reservoir to flow into a coiled copper tubing heat exchanger immersed in the same water tank as the phantom. This ensured that the temperature change, due solely to the flowing water over a 2-min period, was always less than 0.05°C.

Second, fully developed laminar flow conditions were established in the phantom by using an appropriate length of 2-mm diameter plastic tubing entering the phantom. Because the minimum entrance length, for the maximum flow rates used in this study (60 mL/min), was calculated (Streeter 1971) to be 7.3 cm, the 30-cm length of plastic tubing used ensured this condition.

The ultrasonic transducer was clamped in position and was adjusted by a three-way orthogonal axis system that was supported by a solid steel frame above the water tank.

Estimation of perfusion rate in human foetal brains

In animal studies, one method of measuring blood flow is to track the movement of radionuclide-labelled microspheres (of diameter 10 to 15 μm) following arterial injection (Heymann et al. 1977). Blood perfusion rates are usually expressed in terms of the blood flowing (mL min^{-1}) in 100 g of tissue under study (mL min^{-1} 100 g^{-1}). The neonatal pig cerebral perfusion rate, which has been measured by this method (Duggan et al. 2000), was taken as an appropriate model for the human foetal cerebral flow rate. Based on their data, we estimate the human foetal cerebral perfusion rate to be 20 to 30 mL min^{-1} 100 g^{-1}. Furthermore, this estimate concurs with a recent study that modelled the temperature distribution within the newborn infant head (Van Leeuwen et al. 2000), where the cerebral perfusion rate was assumed to be 30 mL min^{-1} 100 g^{-1}. Because the mass of soft tissue-mimicking material contained in the phantoms used in this study was 175 g, this required a flow rate of 35 to 53 mL min^{-1} to achieve perfusion rates of 20 to 30 mL min^{-1} 100 g^{-1}. Despite the limitations of simulating perfusion with liquid flow in a single channel discussed earlier, the usual units for perfusion (mL min^{-1} 100 g^{-1}; NCRP 1992) have been used so as to usefully compare with some of the animal perfusion experiments.

Temperature measurement

In the present study, 10 phantoms were used, each fabricated with a single wall-less channel of diameter 2 mm, but at various distances from the bone mimic. In all cases, one thermocouple was attached to the proximal and another to the distal surface of the bone mimic. For each experiment, after the transducer was set at 9 cm (nominal focal length) from the bone surface, its position was adjusted manually in a plane perpendicular to the transducer axis. This was continued until a maximum temperature rise was detected at the insonated bone surface. This ensured that the thermocouple was aligned to the centre of the US beam. After the specimen temperature had equilibrated with that of the water in the tank at room temperature, heating measurements were taken. The temperature was recorded digitally at 1-s intervals during the period 10 s before insonation, 120 s during insonation and 120 s of cooling. Each temperature elevation produced by the US exposure was measured at least twice for each thermocouple. After all measurements were completed, each phantom was carefully dissected and the distance between the artificial arterial vessel and the bone mimic was measured with a digital vernier calliper (Mitutoyo, Kawasaki, Japan).

Ultrasound dosimetry

The skull bone/brain tissue phantoms were insonated using a single-element 3.5 MHz ultrasonic trans-

ducer of diameter 19.5 mm. A synthesised function generator (Stanford Research Systems, Model DS345, Sunnyvale, CA) provided a series of pulses of duration 5.7 μs and a pulse-repetition rate (PRR) of 8 kHz. These were fed into a Hatfield attenuator (Model 2002, Pascall Electronics Ltd., Isle of Wight, UK), which provided attenuations of 1 to 11 dB, and then to a radiofrequency (RF) power amplifier (ENI, model 2100L, Rochester, NY) of fixed 50-dB gain and band width of 10 kHz to 12 MHz (Fig 2). The power output from the transducer was varied using the Hatfield attenuator and was measured using the Bath power balance (Perkins 1989) to be in the range from 20 $\pm$ 2 mW to 255 $\pm$ 5 mW.

The intensity of the free-field ultrasonic beam in distilled water was deduced from the response of a membrane hydrophone of active diameter 0.5 mm (Model ER175, GEC Marconi, Chelmsford, UK). The captured waveforms were recorded using a digital storage oscilloscope (Model 9310 Dual beam, Lecroy, Chestnut Ridge, NY) sampled at 1 GHz. The temporal average intensity was computed (in steps of 0.5 mm) in the beam and the largest value found was taken as the spatial peak temporal average intensity, I_{SPTA}. The values of the I_{SPTA} intensities were linearly dependent on the acoustic power radiated by the transducer, so that, as the acoustic power varied from 20 mW to 255 mW, the corresponding I_{SPTA} intensities at 90 mm from the front face (nominal focal length) of the transducer varied from 0.22 W cm^{-2} to 2.77 W cm^{-2}. The pulsing conditions used in this study were specifically chosen to avoid nonlinear propagation conditions that may produce additional heating (Bacon and Carstensen 1990; Dalecki et al. 1991; Thomenius 1998).

Although some experiments in this study used the full range of acoustic powers, most experiments concentrated on the ultrasound-induced heating produced by a narrow beam of power 100 mW impinging on the bone phantom at 90 mm from the transducer face. At this location, the US beam had a -6 dB width of 3.1 mm with an intensity of 1.1 W cm^{-2} I_{SPTA} (Fig. 3). This will be referred to as the focussed beam condition at 100 mW of power.

Ultrasonic characteristics of the phantom materials

Measurements of the velocity of ultrasound and insertion power loss, for various thicknesses of T-MM and bone-mimicking material (B-MM), were conducted by using two identical 3 MHz broadband transducers mounted on opposite sides of a small ultrasonic water tank as described by Clarke et al. (1994). The velocity of US at 20°C was 1490 $\pm$ 30 ms^{-1} in the T-MM and 2260 $\pm$ 45 ms^{-1} in the B-MM. The attenuation at 3.5 MHz was 0.11 dB mm^{-1} for the T-MM and 0.7 dB mm^{-1} for the B-MM. This is equivalent to an attenuation coefficient of 0.31 dB cm^{-1} MHz^{-1} for the T-MM and 2 dB cm^{-1} MHz^{-1} for the B-MM, if a linear dependence on frequency is assumed.

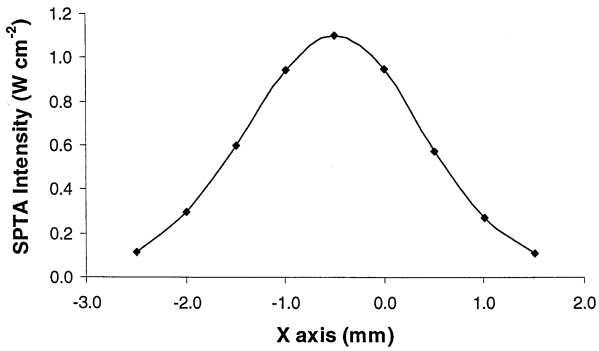

Fig. 3. Cross-axis intensity profile of the ultrasonic beam determined from the hydrophone response in water at an average acoustic power of 100 mW at an axial distance of 90 mm from the transducer (nominal focus).

Statistical analysis

Statistical analyses were carried out by either comparing means with independent-samples *t*-test or determining the association between variables by a linear regression method, as appropriate. The statistical package used in both cases was SPSS for Windows (SPSS, Version 9.0, Chicago, IL). A *p* level of less than 0.05 was required for statistical significance. All results are presented as mean $\pm$ standard error of the mean (SEM).

RESULTS

Ultrasound-induced bone heating with no liquid flow

All 10 foetal phantoms used in the present study possessed identical bone thicknesses (0.5 mm). Hence, with no liquid flow (referred to as the no-flow case), the temperature rise in the foetal-bone phantoms after a fixed ultrasonic exposure was expected to be similar for all 10 specimens. The temperature rises in the proximal and distal surfaces of the bone mimic, after 2-min exposure to the focussed beam condition at a power of 100 mW, were measured to be respectively, 2.76 $\pm$ 0.06°C and 2.54 $\pm$ 0.09°C. A simple experimental study was conducted to examine the effect of a small drop of superglue on the temperature measurement by the thermocouple junction. Identical thermocouples were attached to a piece of 1-mm thick Perspex, one with a small drop of superglue and the other with a drop of acetone that temporarily dissolved the Perspex, while the thermocouple junction was pressed firmly against it. When the Perspex had reset, it secured the thermocouple in place without any need for glue. When the Perspex section was exposed to US, its temperature rose significantly after a

2-min exposure (1°C to 20°C), depending on the incident ultrasonic power. A direct comparison could, thus, be made of the absolute temperature differences with or without the superglue coating. Measurements revealed that the additional heating caused by absorption of the superglue was dependent on the source power and was at most 12% more than the case where no glue was used. When accounting for the absorption artefact at this power level (of 10%), the values are respectively, 2.5 ± 0.1°C and 2.3 ± 0.1°C. The *in situ* values of acoustic power and intensity may be estimated from calculations of the attenuation produced by the overlying tissue layer (approximately 8-mm thick) and bone layer (0.5 mm). The *in situ* values are lower than the free-field values in water by approximately 18% (0.9 dB) for the proximal (upper) bone surface and 25% (1.25 dB) at the distal (or under surface) of the bone due to the additional bone attenuation. The variation between specimens was due to a slight variation of the T-MM (of approximately 2 mm) covering the bone specimens. This small thickness variation represents a difference in the ultrasonic energy deposited on the bone section of 0.22 dB (or 5%). Taking into account the typical uncertainty in a hydrophone measuring system to be 22% in the value of I_{SPTA} at the 95% confidence level (Preston 1991), this difference is well within the uncertainty in the intensity measurement. The temperature rises measured at the proximal and distal surfaces, together with the standard errors, show that the variation due to the overlying T-MM thickness had a negligible effect on the measurements.

Effect of liquid flow on the ultrasound-induced bone heating

The effect of liquid flow (40 mL min^{-1}, equivalent to a perfusion rate of 23 mL min^{-1} 100 g^{-1}) on the rate of temperature rise for a bone-tissue phantom in which the single flow channel was 1.5 mm from the bone mimic (referred to as the flow case) is shown in Fig. 4. The results were obtained from 3 specimens with repeated measures (25 in all), which were exposed to the focussed ultrasound beam of power 100 mW. Although temperature measurements were made for both the proximal and distal surfaces of the bone mimic, only the distal bone-surface temperatures (closer to the flow channel) are recorded in Fig. 4. The temperatures at the distal bone surface are more biologically significant because they simulate what occurs at the skull bone-brain interface *in vivo*. The proximal bone-surface temperatures (which are not shown) exhibit a similar trend, with a reduced cooling for the case in which a liquid flows. The error bars represent the SEM of these measurements, indicating consistent data.

In both no-flow and flow cases, the temperature increased to a significant percentage of its 2-min temperature rise within the first 30 s of insonation. In the no-flow case, this was 82% and in the flow case, it was 88% of the 2-min temperature rise. The temperature increase after 2 min for the no-flow case was 2.91°C and 2.52°C for the flow case. Hence, the liquid flow produced a reduction in the bone-mimic temperature elevation (or cooling) of 13.4% at this 1.5 mm bone-channel spacing. Furthermore, the difference between the flow and no-flow cases was statistically significant (at the $p < 0.05$ level) after 18 s of US exposure. Similar heating curves were obtained at other bone–channel separations with the most effective cooling at small separations, as discussed in a later section. The difference between the flow and no-flow curves became statistically significant at different times that depended on the bone–channel separation as shown in Table 2. Although, to some extent, the variation in the times of detecting a difference is partly dependent on the "noise" in the experiment, it also gives an indication of how quickly liquid flow effects become important.

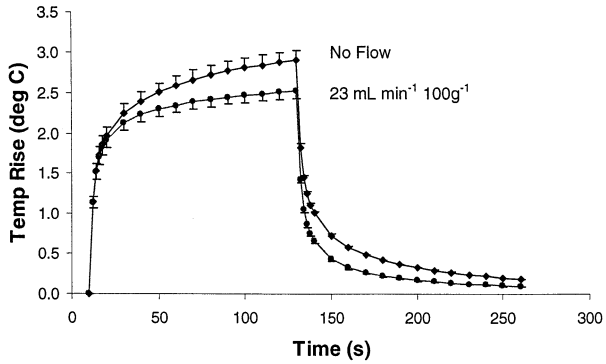

Fig. 4. The heating curves for the bone surface close to the flow channel when exposed to a focused US beam of power 100 mW. The upper curve shows the heating with no flow and, the lower curve, the heating curve for a flow equivalent to a perfusion of 23 mL min^{-1} 100 g^{-1}. These results refer to specimens where the flow channel was separated from the bone mimic by 1.5 mm of tissue-mimicking material, measured at the lower (or distal) bone surface. The error bars represent the SEM of the measurements.

Table 2. The time required before the difference between the flow and no-flow heating curves for various bone-channel spacings becomes significant at the $p < 0.05$ level

Bone-channel spacing (mm)	Time for statistical significance (s)
1	4
1.5	18
3	90

The temperature was measured at the distal bone surface (close to the flow channel) during exposure to the focussed beam condition at a power of 100 mW.

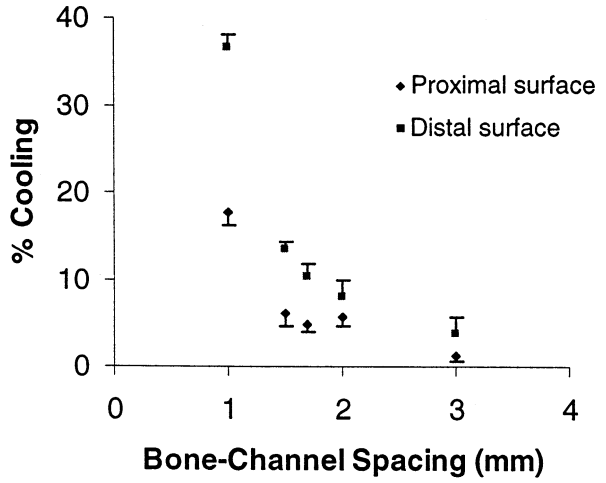

Fig. 5. The percentage cooling as a function of the bone-channel spacing for the proximal and distal bone surfaces after 2-min exposure to an ultrasonic focused beam of power 100 mW.

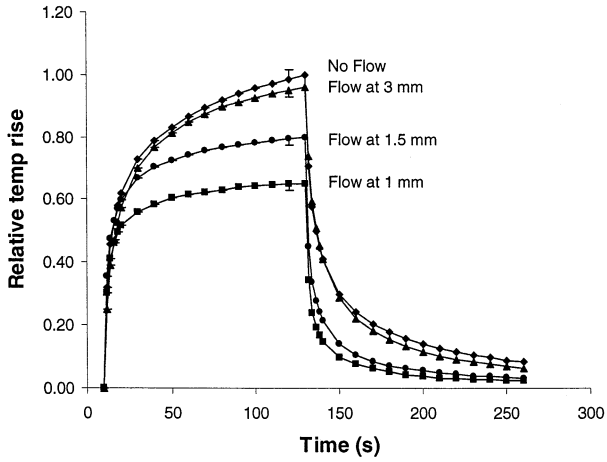

Fig. 6. The heating curves for no-flow and flow cases at various bone-channel separations when the distal bone surface is exposed to a focussed beam of US of power 100 mW. The curves are normalised with respect to the no-flow case. The error bars at 110 s give the SEM.

In both the flow and no-flow cases, the temperature fell immediately the US was switched off. The fall in temperature following cessation of the US was more rapid under flow conditions and, in both flow and no-flow cases, the temperature returned to within 0.2°C of the initial equilibrium temperature within 2 min.

Cooling as a function of the bone-channel spacing

In this series of experiments, a flow rate of 35 ± 9 mL min^{-1} (equivalent to a perfusion rate of 20 ± 5 mL min^{-1} 100 g^{-1}) was maintained in all phantoms that contained a single channel at various distances from the bone mimic. Figure 5 shows a graph of the cooling due to liquid flow as a function of the bone-channel separation for both proximal and distal bone surfaces after 120 s of focussed insonation at 100 mW power. At 1 mm bone-channel separation, perfusion produces a 37% cooling at the distal surface of the bone mimic (closer to the channel) and 18% at the proximal surface. The cooling effect of liquid flow reduces dramatically with increasing separation until, at 3 mm, the cooling is approximately 4% at the distal bone surface and a little over 1% at the proximal bone surface.

Another way of illustrating the dramatic effect of changing the bone-flow channel separation on the cooling efficiency of the liquid flow is shown by comparing the bone heating curves. Figure 6 shows the heating curves, measured at the distal bone surface, for no flow as well as those flow cases for bone-channel separations of 1 mm, 1.5 mm and 3 mm of T-MM. All heating curves have been normalised relative to the no-flow case, for ease of comparison. The cooling effect of liquid flow is most efficient at small bone-channel separations and is negligible by a distance of 3 mm. The error bars shown give the SEM of measurements after 110 s of insonation.

Cooling as a function of acoustic power

The cooling effect of liquid flow (expressed as a percentage) in a single channel was measured at the distal bone surface, 1.5 mm away from the channel, as a function of acoustic power for a variety of perfusion rates, two of which are shown in Fig. 7.

The error bars shown represent the SEM for each of these perfusion rates. A linear regression analysis of these results revealed no association between the per-

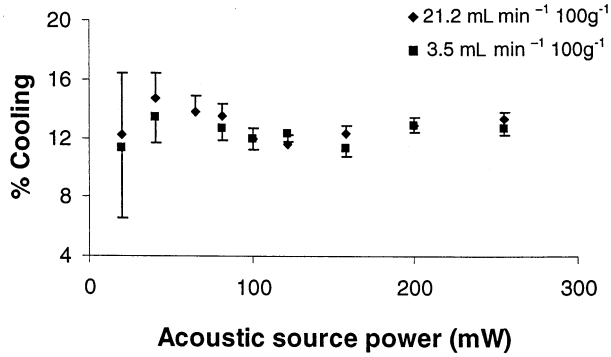

Fig. 7. The percentage cooling due to liquid flow as a function of the acoustic source power at two different perfusion rates for specimens with a bone-channel separation of 1.5 mm. The temperatures were measured at the distal bone surface at the focus of the US beam. The error bars represent the SEM of the measurements.

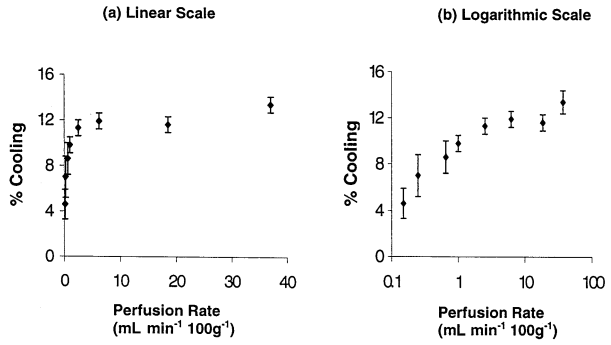

Fig. 8. The variation of the percentage cooling as a function of the perfusion rate after a 2-min exposure to an US beam of power 100 mW, a −6 dB beam width of 3.1 mm and intensity of 1.1 W cm^{-2} I_{SPTA}. Measurements were made at the distal bone surface for a bone-channel separation of 1.5 mm. (a) The relationship for the perfusion rate drawn on a linear scale, and (b) the case for the perfusion rate drawn on a logarithmic scale.

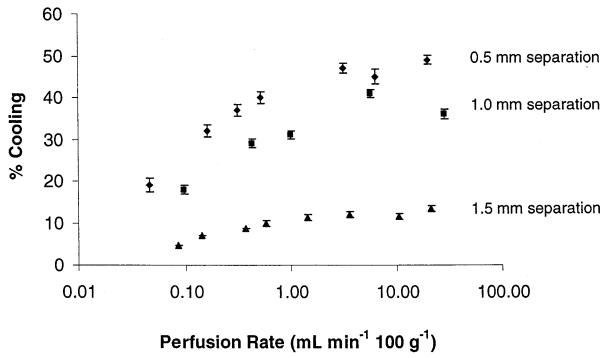

Fig. 9. Graph of the percentage cooling vs. perfusion rate for bone-channel spacings of 1.5 mm, 1.0 mm and approximately 0.5 mm. In all cases, the specimens were exposed to a focused beam of power 100 mW and the temperatures measured at the distal bone surface, and the "plateau effect" is evident.

centage cooling and the acoustic source power for both perfusion rates ($p > 0.06$ for a perfusion rate of 21 mL min^{-1} 100 g^{-1} and $p > 0.72$ at a rate of 3.5 mL min^{-1} 100 g^{-1}). This behaviour (of cooling being independent of the acoustic source power) was replicated at other separation distances between the liquid flow channel and the bone mimic (0.5 mm to 2 mm), as well as for the proximal bone surface.

Cooling vs. perfusion rate for a single-flow channel

Using a single-flow channel at a separation of 1.5 mm from the bone mimic, the cooling effect was measured for the distal bone surface as a function of the perfusion rate during exposure to the focussed beam condition at a power of 100 mW (Fig. 8). The amount of cooling increases as the perfusion rate increases up to about 5 mL min^{-1} 100 g^{-1}, after which it saturates to a constant value for higher perfusion rates. This plateauing effect was also detected for other bone-channel spacings at approximately the same perfusion rate (5 mL min^{-1} 100 g^{-1}). This behaviour is illustrated in Fig. 9, which shows a comparison of the percentage cooling vs. perfusion rate for the distal bone surface at three different bone-channel spacings.

DISCUSSION

The temperature rise measured for the proximal surface of the no-flow bone phantom (simulating the outer part of the skull bone) in this study was 2.5 ± 0.1°C after a 2-min exposure to the focussed beam conditions with a free-field in water intensity of 1.1 W cm^{-2} I_{SPTA}. The *in situ* value of the intensity due to the overlying tissue layer was 18% lower with a value of 0.90 W cm^{-2} I_{SPTA}. This temperature rise may be compared with that measured by Doody et al. (1999) with a thermocouple attached to the outer surface of human foetal vertebrae that were exposed to US of intensity of 0.53 ± 0.16 W cm^{-2} I_{SPTA}. This intensity was essentially the *in situ* value because the human foetal vertebrae were embedded in agar, which attenuated the US beam by less than 0.2% (Doody et al. 1999). For the case of a 39-week gestational age human vertebra, Doody and colleagues measured a temperature rise of 1.45 ± 0.1°C after a 2-min US exposure. Taking the 2.5°C temperature rise in this study and scaling it linearly to what would be expected for the lower intensity (0.53 W cm^{-2} instead of our *in situ* estimate of 0.90 W cm^{-2}), yields a temperature rise of 1.5°C. This compares favourably with the 1.45 ± 0.1°C obtained in the Doody experiment, considering the large intrinsic error in the measurement of intensity and the use of slightly different US field conditions in the two experiments. The vertebrae were placed at a distance of 80 mm from the transducer face where the −6-dB beam width was 2.9 mm whereas, in this study, the bone phantoms were positioned at a distance of 90 mm from the transducer, where the −6 dB beam width was 3.1 mm. This suggests that the phantom material used in this study is an acceptable simulator of the ultrasonic heating of human foetal bone. This is not surprising because the thermal properties of the bone-mimicking material are closely matched to those of ideal foetal bone. It should be noted that the acoustic properties, such as acoustic impedance and attenuation coefficient, are both lower than the ideal foetal bone values.

The percentage cooling achieved by fluid flow in a single channel near an ultrasonically heated bone target varied considerably with the thickness of tissue-mimicking material between the bone and the flow channel (Fig 5). The variation of the perfusion rate used in this study (20 ± 5 mL min^{-1} 100 g^{-1}) was not important because

the flow-induced cooling was independent of perfusion rate, after it was above about 5 mL min^{-1} 100 g^{-1} (Fig. 8). A similar reduction in the perfusion-induced cooling effect of ultrasonically heated thigh muscles in greyhound dogs was found (Dorr and Hynynen 1992) when the temperature was measured at increasing distances from the femoral artery. Hume et al. (1979) measured the influence of blood flow on the temperature distribution of exteriorised mouse intestine while a loop of exteriorised jejunum was immersed in a hot bath. Their histologic and thermometric data suggested that major blood vessels influenced the tissue temperature over a distance of approximately 2 mm. These results provide convincing support for the hypothesis that the proximity of the perfusing channel has a very significant effect on the cooling effect of perfusion. The large variations observed in the perfusion-induced cooling (Table 1) may, at least partly, be explained by assuming that the main cerebral vessels were at different distances from the insonated sections of bone in the various animal models. These would include the superficial branches of the major cerebral and meningeal arteries (Moore and Dalley 1999). The perfusion-induced cooling for the sphenoid bone (Horder et al. 1998a) was significantly greater than that of all the other heated bone sites. This is perhaps not surprising because the sphenoid bone, located at the base of the brain case, contains a large air sinus, is relatively well perfused and is related closely to the cavernous sinuses and the internal carotid arteries (Williams and Warwick 1989). The blood supply to the adjacent pituitary gland is rich with at least eight branches arising from a number of other cerebral vessels, which then drain into the cavernous sinuses *via* numerous veins. The internal carotid artery, which lies beside the sphenoid bone in the form of an S curve, is a major supplier of blood to the brain. Hence, these anatomical structures provide an efficient heat sink close to the sphenoid bone.

It is interesting to note that the cooling effect of liquid flow at the proximal surface, where the TIB is estimated, is approximately half as efficient as at the distal bone surface.

The times required for a statistical difference between the flow and no-flow cases decreased as the bone-channel separation decreased (Table 2). These data may be interpreted in another way by stating that liquid flow plays an important role in the flow-induced cooling within 4 s of insonation for a bone-channel separation of 1 mm. In a similar way, flow-induced cooling is important within 18 s or 90 s of insonation for bone-channel separations, respectively, of 1.5 mm and 3 mm. The theoretical study by Kolios et al. (1996) on ultrasonic lesion formation predicted that blood flow would play a significant role within 8 s of ultrasonic exposure. In an experimental study on lesion data in rabbit brain, Vykhodtseva et al. (1994) confirmed that the lesion size was independent of perfusion for exposure times of 2 s. These times are comparable with the time of 4 s in this study, which occurred at a bone-channel separation of 1 mm.

The cooling effect of liquid flow was found to be independent of the acoustic source power at a number of different perfusion rates. This is not surprising because heat from the insonated bone target is conducted through the tissue-mimicking material between the bone and channel, after which it is convected away along the channel. As the acoustic power is increased, so also is the temperature difference between the bone phantom and the flow channel, thus producing a proportional increase in the heat conducted in the tissue-mimicking material and convected by water flowing in the channel. Because the thermal resistance of a given thickness of tissue material is constant, this then produces the same cooling percentage. It is merely a manifestation of Newton's law of cooling (Incropera and Dewitt 2002), where a greater temperature difference produces a greater thermal current due to conduction in the tissue-mimicking material and convection in the adjacent flowing liquid layer.

The flow-induced percentage cooling was found to increase as the perfusion rate increased to a rate of approximately 5 mL min^{-1} 100 g^{-1}, after which it reached a plateau and was approximately constant with a further increase in perfusion rate. In the present study, a perfusion rate of 5 mL min^{-1} 100 g^{-1} is equivalent to a flow rate of 8.75 mL/min which, for the 2-mm diameter channel, corresponds to a flow velocity of 4.6 cm s^{-1}. This result suggests that the flowing liquid needs to be flowing slowly enough (less than about 5 cm s^{-1}) to allow it sufficient time to absorb heat conducted across the tissue and, subsequently, convect it away from the heated bone site. This finding is supported by an experimental study (Torell and Nilsson 1978), in which hot water was forced into a 2-mm diameter channel at the centre of a Perspex block. Temperatures at the inlet and outlet were measured by calibrated thermistors. The temperature reduction between inlet and outlet (or cooling) increased with flow velocity and was found to plateau to a constant value at a velocity of approximately 5 cm s^{-1} (Torell and Nilsson 1978). A similar plateau effect in the cooling curve was reported in the study of ultrasonically heated greyhound thigh muscles (Dorr and Hynynen 1992). They found that the flow rate had a significant effect on the cooling curve when the flow was increased from 0% to 25% of the full flow rate, with negligible effect at higher rates. In the present study, the plateau effect commences at about 20% of the assumed full flow rate. In addition, this plateau phase was also detected in the neonatal pig study (Duggan et al. 2000), where only a small increase (10%) in the perfusion-induced cooling was measured, even though the perfusion rate was in-

creased by a factor of three during hypoxic and hypercarbic conditions.

CONCLUSION

This study demonstrates the usefulness of employing a very simple model to evaluate the factors that affect the cooling produced by a liquid flowing in a single channel near an ultrasonically heated foetal skull phantom. It is acknowledged that the cooling effect of homogeneous *in vivo* perfusion is not the same as cooling by a single large vessel, as used in the present study. Nevertheless, it has confirmed and strengthened previous findings of both animal experiments and computer simulations that further the understanding of the variation in the perfusion-induced cooling percentages previously reported. This study has established that, when a narrow ultrasonic beam heats a bone target, the cooling effect of liquid flow in a single simulated arterial vessel is independent of the acoustic source power. Furthermore, the cooling is more effective at shorter bone-channel distances and initially increases with flow rate but then saturates to a constant value.

The bone-mimicking material used in this study (high-density polyethylene) was a reasonable phantom material to simulate the ultrasonic heating of human foetal bone.

Acknowledgments—The authors thank Cathy Dyer, from the Medical Ultrasonics laboratory in the University of Bath, for her technical expertise in producing the tissue-mimicking material used in the skull bone/brain tissue phantoms. They also thank Dr. Nic Jayasundere for his helpful comments and suggestions with regard to the phantom designs, and Dr. Mark Cahill for the measurement of the ultrasonic intensities. The authors are grateful to the University of Sydney for granting this study leave period to allow G. Vella to complete this work at the University of Bath. The authors acknowledge and appreciate the support provided by all institutions involved (University of Sydney, University of Bath, Royal United Hospital and CSIRO) in this international collaborative project.

REFERENCES

Abbott JG. Rationale and derivation of MI and TI—A review. Ultrasound Med Biol 1999;25:431–441.

AIUM/NEMA (American Institute of Ultrasound in Medicine/National Electrical Manufacturers Association. Standard for real-time display of thermal and mechanical acoustic output indices on diagnostic ultrasound equipment. Rockville, MD: AIUM Publications, 1992.

Andrews M, Webster M, Fleming JE, McNay MB. Ultrasound exposure time in routine obstetric scanning. Br J Obstet Gynecol 1987; 94:843–846.

Bacon DR, Carstensen EL. Increased heating by diagnostic ultrasound due to nonlinear propagation. J Acoust Soc Am 1990;88:26–34.

Bacon DR, Shaw A. Experimental validation of predicted temperature rises in tissue mimicking material. Phys Med Biol 1993;38:1647–1659.

Barnett SB. Ultrasound safety in obstetrics: What are the concerns? Ultrasound Q 1996;13:228–239.

Barnett SB. Ultrasound-induced heating and its biological consequences. In: Ter Haar G, Duck FA, eds. The safe use of ultrasound in medical diagnosis. Oxford: BMUS and BIR, 2000:32–41.

Barnett SB. Intracranial temperature elevations from diagnostic ultrasound. Ultrasound Med Biol 2001;27:883–888.

Barnett SB, ed. for WFUMB (World Federation of Ultrasound Med Biol). Symposium on safety, and standardisation of ultrasound in medicine. Update on thermal bioeffects issues. Ultrasound Med Biol 1998;24(Suppl. 1):1–10.

Bentley RE. Theory and practice of thermoelectric thermometry. Singapore: Springer-Verlag, 1998:29.

Bettelheim D, Deutinger J, Bernaschek G. Fetal sonographic biometry. New York: Parthenon Publishing Group, 1997:2–31.

Billard BE, Hynynen K, Roemer RB. Effects of physical parameters on high temperature ultrasound hyperthermia. Ultrasound Med Biol 1990;16:409–420.

Carstensen EL, Child SZ, Norton S, Nyborg WL. Ultrasonic heating of the skull. J Acoust Soc Am 1990;87:1310–1317.

Clarke AJ, Evans JA, Truscott JG, Milner R, Smith MA. A phantom for quantitative ultrasound of trabecular bone. Phys Med Biol 1994; 39:1677–1687.

Crezee J, Lagendijk JJW. Temperature uniformity during hyperthermia: The impact of large vessels. Phys Med Biol 1992;37:1321–1337.

Dalecki D, Carstensen EL, Parker KL, Bacon DR. Absorption of finite amplitude focused ultrasound. J Acoust Soc Am 1991;89:2435–2447.

Dickinson RJ. Thermal conduction errors of manganin-constantan thermocouple arrays. Phys Med Biol 1985;30:445–453.

Doody C, Porter H, Duck FA, Humphrey VF. In vitro heating of human fetal vertebra by pulsed diagnostic ultrasound. Ultrasound Med Biol 1999;25:1289–1294.

Dorr LN, Hynynen K. The effects of tissue heterogeneities and large blood vessels on the thermal exposure induced by short high-power ultrasound pulses. Int J Hypertherm 1992;8:45–59.

Duck FA. Physical properties of tissue, a comprehensive reference book. London: Academic Press, 1990.

Duck FA, Henderson J. Acoustic output of modern ultrasound equipment: Is it increasing?. In: Barnett SB, Kossoff G, eds. Safety of diagnostic ultrasound. New York: Parthenon Publishing Group, 1998:15–26.

Duggan PM, Murcott MF, McPhee AJ, Barnett SB. The influence of variations in blood flow on pulsed Doppler ultrasonic heating of the cerebral cortex of the neonate. Ultrasound Med Biol 2000;26:647–654.

England MA. Life before birth, 2nd ed. London: Mosby Wolfe, 1996: 202.

Fry W, Fry R. Determination of absolute sound levels and acoustic absorption coefficients by thermocouple probes—Theory. J Acoust Soc Am 1954;26:294–310.

Goss SA, Cobb J, Frizzell L. Effect of beamwidth and thermocouple size on the measurement of ultrasonic absorption using the thermoelectric technique. IEEE Ultrason Symp Proc 1977;1:206–211.

Henderson J, Willson J, Jago R, Whittingham T. A survey of the acoustic outputs of diagnostic equipment in current clinical use. Ultrasound Med Biol 1995;21:699–705.

Heymann MA, Payne BD, Hoffman JI, Rudolf AM. Blood flow measurements with radionuclide-labelled particles. Progr Cardiovasc Dis 1977;20:55–79.

Horder MM, Barnett SB, Vella GJ, Edwards MJ. Effect of pulsed ultrasound on the sphenoid bone temperature and the heart rate in guinea-pig foetuses. Early Human Devel 1998a;52:221–233.

Horder MM, Barnett SB, Vella GJ, et al. In vivo heating of the guinea-pig fetal brain by pulsed ultrasound and estimates of the thermal index. Ultrasound Med Biol 1998b;24:1467–1474.

Hume SP, Robinson JE, Hand JW. The influence of blood flow on temperature distribution in the exteriorized mouse intestine during treatment by hyperthermia. Br J Radiol 1979;52:219–222.

Incropera FP, Dewitt DP. Fundamentals of heat and mass transfer, 5th ed. New York: John Wiley & Sons, 2002.

Kolios MC, Sherar MD, Hunt JW. Blood flow cooling and ultrasonic lesion formation. Med Phys 1996;23:1287–1298.

Kolios MC, Worthington AE, Holdsworth DW, Sherar MD, Hunt JW. An investigation of the flow dependence of temperature gradients

near large vessels during steady state and transient tissue heating. Phys Med Biol 1999;44:1479–1497.
Kuhn PK, Christensen DA. Influence of temperature probe sheathing materials during ultrasonic heating. IEEE Trans Biomed Eng 1986; 33:536–538.
Lagendijk JJW. The influence of bloodflow in large vessels on the temperature distribution in hyperthermia. Phys Med Biol 1982;27: 17–23.
Law YF, Johnston KW, Routh HF, Cobbold RSC. On the design and evaluation of a steady flow model for Doppler ultrasound studies. Ultrasound Med Biol 1989;15:505–516.
Lewinsky R, Farine D, Knox-Ritchie J. Transvaginal Doppler assessment of the foetal cerebral circulation. Obstet Gynecol 1991;78: 637–640.
Madsen EL, Zagebski JA, Frank GR. Oil-in-gelatin dispersions for use as ultrasonically tissue-mimicking materials. Ultrasound Med Biol 1982;8:277–287.
Martin CJ, Law AN. Design of thermistor probes for measurement of ultrasound intensity distributions. Ultrasonics 1983;21:85–90.
McCowan LM, Duggan PM. Abnormal internal carotid and umbilical artery Doppler studies in the small for gestational age fetus predicts an adverse outcome. Early Hum Dev 1992;30:249–259.
Moore KL, Dalley AF II. Clinically oriented anatomy, 4th ed. Philadelphia: Lippincott Williams and Wilkins, 1999:874–898.
Ohtsuki F. Developmental changes of the cranial bone thickness in the human fetal period. Am J Phys Anthropol 1977;46:141–154.
NCRP (National Council on Radiation Protection, and Measurements). Exposure criteria for medical diagnostic ultrasound: I. Criteria based on thermal mechanisms, Report No. 113. Bethesda, MD: NCRP Publications, 1992:53–55.
Pay NM, Shaw A, Bond AD. Evaluation of potential bone mimicking materials for ultrasound thermal test objects NPL report CMAM 10, Teddington, UK: National Physical Laboratory, 1998.
Perkins MA. A versatile force balance for ultrasound power measurements. Phys Med Biol 1989;34:1645–1651.
Preston RC, ed. Output measurements for medical ultrasound. London, UK: Springer-Verlag, 1991.
Rickey DW, Picot PA, Christopher DA, Fenster A. A wall-less vessel phantom for Doppler ultrasound studies. Ultrasound Med Biol 1995;21:1163–1176.
Shaw A, Preston RC, Bacon DR. Perfusion corrections for ultrasonic heating in nonperfused media. Ultrasound Med Biol 1996;22:203–216.
Schultz DM, Giordano DA, Schultz DH. Weights of organs of fetuses and infants. Arch Pathol 1962;74:80–86.
Siebert J, Glasier C, Leithiser R, Kinder D, Tennant A. Transcranial Doppler using standard duplex equipment in children. Ultrasound Q 1990;8:167–196.
Streeter VL. Fluid mechanics. New York: McGraw-Hill, 1971.
Thomenius KE. Impact of nonlinear propagation on temperature distributions caused by diagnostic ultrasound. IEEE Ultrason Symp Proc 1998;2:1409–1413.
Torell LM, Nilsson SK. Temperature gradients in low-flow vessels. Phys Med Biol 1978;23:106–117.
Van Leeuwen GM, Hand JW, Lagendijk JJ, Azzopardi DV, Edwards AD. Numerical modeling of the temperature distributions within the neonatal head. Pediatr Res 2000;48:351–356.
Vella GJ, Humphrey VF, Duck FA, Barnett SB. Ultrasound-induced heating in a foetal skull bone phantom and its dependence on beam width and perfusion. Ultrasound Med Biol 2003;29:779–788.
Vykhodtseva NI, Hynynen K, Damianou C. Pulse duration and peak intensity during focussed ultrasound surgery: Theoretical and experimental effects in rabbit brain in vivo. Ultrasound Med Biol 1994;20:987–1000.
Waterman FM, Dewhurst MW, Fessenden P, et al. RTOG quality assurance guidelines for clinical trials using hyperthermia administered by ultrasound. Int J Radiat Oncol Biol Phys 1991;20:1099–1107.
Williams PL, Warwick R, eds. Gray's anatomy, 37th ed. Edinburgh: Churchill Livingston, 1989.
Wu J, Chase JD, Zhu Z, Holzapfel TP. Temperature rise in a tissue-mimicking material generated by unfocused and focused ultrasonic transducers. Ultrasound Med Biol 1992;18:495–512.